PERGAMON

International Journal of Heat and Mass Transfer 42 (1999) 1189–1204

International Journal of HEAT and MASS TRANSFER

Boiling liquid nitrogen heat transfer in channels with porous copper inserts

Tuncer M. Kuzay*, Jeffrey T. Collins and Joshua Koons[1]

Experimental Facilities Division, Advanced Photon Source, 9700 South Cass Avenue, Argonne National Laboratory, Argonne, IL 60439, U.S.A.

Received 7 May 1998; in final form 27 July 1998

Abstract

Copper mesh, compressed and formed into porous matrices of various shapes and sizes, has been routinely used in high heat load/flux component cooling with water at the Advanced Photon Source (APS) to significantly enhance the heat transfer performance. Now the same mesh configuration is being applied to the cryogenic cooling of optical components, such as the monochromators, mirrors and multilayers with liquid nitrogen in single phase. Two-phase heat transfer is avoided to prevent flow-induced noise (vibrations and jitter) in the ultrasensitive optical components. Hence there is a great need to understand the limits of single-phase heat transfer with copper mesh using liquid nitrogen. Recently an extensive experimental program has been undertaken to investigate the heat transfer limits in conductive porous matrices with liquid nitrogen as the coolant. This paper presents the data obtained, compares the data with existing single- and two-phase correlations, and interprets the results for cryo-cooled optical component cooling applications.

Nomenclature

c_p specific heat [J kg^{-1} K^{-1}]
D inner diameter of tube [m]
d pore size [m]
d_f fiber diameter [m]
f friction coefficient
G mass flow rate [kg min^{-1}]
h heat transfer coefficient [W m^{-2} K^{-1}]
k thermal conductivity [W m^{-2} K^{-1}]
LN2 liquid nitrogen
l length of a tube [m]
Nu Nusselt number
p pressure [Pa]
Pe Peclet number
q''_w wall heat flux [W m^{-2} K^{-1}]
Re Reynolds number
t time [sec]
T temperature [°C]
u superficial velocity [m s^{-1}]
u_o superficial porous core velocity [m s^{-1}].

Greek symbol
ε porosity.

Subscripts
eff effective
f fluid phase
i inlet
l saturated liquid
m mean (bulk)
s solid phase
sat saturation
w inner wall.

1. Introduction

Porous inserts have been used for enhancing heat transfer in cooling channels for high heat flux applications [1–6]. At the Advanced Photon Source (APS) at Argonne National Laboratory (ANL), the heat flux from the powerful APS insertion-device magnets imposed on the

* Corresponding author. Tel.: 001 630 252 3084; fax: 001 630 252 9350; e-mail: kuzay@aps.anl.gov
[1] Summer student participant, Bradley University

0017–9310/98/$ - see front matter
PII: S0017–9310(98)00248–8

X-ray beamline components is of the order of 600 W mm^{-2} at normal incidence. Through innovative grazing-angle engineering, the actual heat flux impinging on the beam-interacting components is reduced to under 30 W mm^{-2}, which is manageable using high temperature materials and advanced cooling concepts. In the mechanical stops and shutters of the beamlines, the cooling medium is normally water in single phase. Two-phase cooling is avoided for assured reliability and mitigation of vibrations. The high heat flux and heat load levels handled by the x-ray components require highly enhanced cooling methods wherever appropriate to assure long-term structural integrity of the components as well as to minimize use of expensive deionized cooling water in the facility. For high heat transfer enhancement, we have chosen the use of rolled and compressed copper mesh inserts in the cooling channels [7–9]. Extensive research to optimize the cooling enhancement and pressure drop and to minimize deionized water use in single phase resulted in the selection of an enhanced heat transfer coefficient of the order of 2.5–3.0 W $cm^{-2} K^{-1}$. Compared to plain channels of the same size, this enhancement represents, on an average, a seven-fold increase in the value of the heat transfer coefficient while there is an almost 8 to 1 reduction in the required amount of deionized water. While the cooling of the mechanical components on the beamlines is satisfied with the scheme described above using water as the coolant, cryogenic cooling of the optical components with similar conductive mesh offers distinct advantages [8, 10]. Because the optical components exhibit very low tolerance to flow-induced vibrations and jitter, the use of porous media in the flow channels of such optical elements was suggested. The low flows sufficient for an efficient porous media heat transfer operation, coupled with the intrinsic turbulence-reducing characteristics of such media, achieve a highly quiet but very effective cooling in these components. Optical components, exemplified by the monochromator crystals and mirrors, typically use materials such as single-crystal silicon or diamonds, natural or man-made, and specialty ceramics and semiconductors. It is widely known that silicon and especially diamond exhibit very desirable thermo-physical properties at cryogenic temperatures, particularly with liquid nitrogen (LN2). At cryogenic temperatures, the inherent high thermal conductivity of the optical materials as well as the low thermal expansion coefficient (nearly zero for diamond) result in very low thermal distortions in the components, which is very desirable for optical performance [11–19]. In cooling of the optical components in high heat flux applications, liquid nitrogen, as a coolant, is an attractive economic choice as it is abundant and inexpensive. On the negative side, cryogenics, in general, will reach boiling at a lower heat flux. They exhibit an undesirable rapid and uncontrollable vapor blanketing upon boiling due to small saturation temperature differences. Porous inserts are known to offset some of the negative aspects of two-phase heat transfer in cryogenically cooled plain-tube channels. The inserts are known to cause larger saturation temperature differences in the cooled channel; hence boiling is harder to start in a channel with a porous insert. On the other hand, the bulk temperature difference in the fluid cross section is smaller in a porous medium particularly for metallic inserts, compared to a plain-channel flow. Hence while the cryogenically cooled plain-channels can operate in a subcooled boiling mode, the porous-insert channels are known to rapidly transform from onset of boiling (OOB) to rapid full voiding. Hence the classic onset of nucleate boiling (ONB) followed by a steady nucleate boiling does not generally exist in channels with porous inserts. As such, we will use the terminology OOB throughout in place of the conventional ONB. Only if acoustically benign and maintainable in a steady fashion, is subcooled convective boiling permissible in operations. Otherwise, single-phase cryogenic cooling is the preferred method. Thus, one needs to know precisely the initiation of boiling and transition through the subcooled boiling with the liquid nitrogen. The limits of subcooled nucleate boiling in porous media are quite complicated for any modeling or extraction from existing boiling heat transfer correlations. Therefore an experimental program was undertaken to generate information that can be used in practice to estimate heat transfer and associated pressure losses.

The focus of the experimental program has been in determining the limiting heat flux before uncontrolled boiling can occur in a tube filled with a porous insert under LN2 cooling. Data were generated with tubes at various porosities, brazed to or in mechanical contact with the uniform heat flux boundary. An attempt was made to predict whether the considered heat flux conditions could be safely used along with the prescribed restrictive operating conditions on the inlet temperature, operating pressure, and maximum allowable coolant flow rate. This analysis was based on a synthesis of the information that was extracted from the investigations performed to date on forced convective boiling in plain tubes and tubes/channels with porous inserts.

2. Experimental setup

Single-phase liquid nitrogen is supplied to the test section at variable flow rate and pressure by an APS designed liquid nitrogen pumping system. The pumping system comprises a dewar, a variable speed centrifugal pump, an integral heat exchanger, and vacuum-insulated valves and transfer lines. The flow rate is measured downstream of the pump by a Coriolis mass-flow meter. The flow rate is adjustable from about 1–15 kg min^{-1}. The inlet pressure to the pump is adjustable up to 150 psig. The closed-loop, pressure subcooled LN2 pumped through

the test section returns to the dewar vessel where it circulates through the heat exchanger submerged in a bath of atmospheric LN2. The atmospheric LN2 boils off, removing heat from the pumped liquid, thereby maintaining a constant fluid inlet temperature to the test section of about 80 K. An auxiliary dewar maintains the inventory of LN2 in the bath. In most cases in the tests, the inlet pressure of the LN2 is kept at about 5.5 bars (80–85 psig) giving a saturation temperature of about 87–90 K.

The test section is in a vacuum tank, which is kept normally at 10^{-2} torr. The test tubes are all similarly prepared and instrumented. The test tubes, schematically shown in Fig. 1, are made of oxygen-free high conductivity (OFHC) copper. All test tubes are the same with 12.7 mm (1/2 in.) OD and 9.53 mm (3/8 in.) ID. Two Kapton-encapsulated thermofoil heaters are continuously wrapped around the tube with about 1.6 mm spacing in between the wraps. Each heater has been rated at 250 W heating capacity. Miniature copper–constantan thermocouples (TC) with 0.005 ml wire diameters are attached to the copper surface using an indium-eutectic solder at six locations.

Rolled and uniformly compressed copper mesh is used in the flow channel to enhance heat transfer. These copper mesh inserts were made from what is called 8×8 U.S. standard sieve (8×8 openings in^2) with 0.15 mm (0.0126 in.)-diameter wire woven fabric. After rolling a cut piece of the copper fabric around a 4–40 threaded stainless steel rod, the mesh is uniformly compressed to shape in an in-house designed and automated mesh-making machine. The initial mesh fabric size processed in compression determines the desired porosity. At the APS, the high heat flux components use $\varepsilon = 76\%$ porous tubes in the optimized design for single-phase deionized water cooling. The table insert in Fig. 1 lists the tube types tested in the current phase of the studies. Three copper mesh porosities at 76, 82 and 88% are used, with two tubes in each case, one with brazed and another with non-brazed (mechanical wall contact) mesh. Tubes are attached to the flexible flow lines via synthetic couplings to reduce axial heat losses.

Each tube is approximately 343 mm (13.5 in.) in total length; the copper mesh inside is 305 mm (12 in.) long. The heated length of the tube is 203 mm (8 in.) long. Therefore an unheated porous flow entry length of about 50.8 mm (2.0 in.) exists in each test tube. Then a 20.3 cm long heated section follows, ending with another unheated porous section, 50.8 mm (2.0 in.) long. Uniform ohmic heat was applied via a 2 kW capacity-regulated DC power supply. The hydraulic diameter length (L/D_h) of the test tubes is approximately 36 mm and the heated

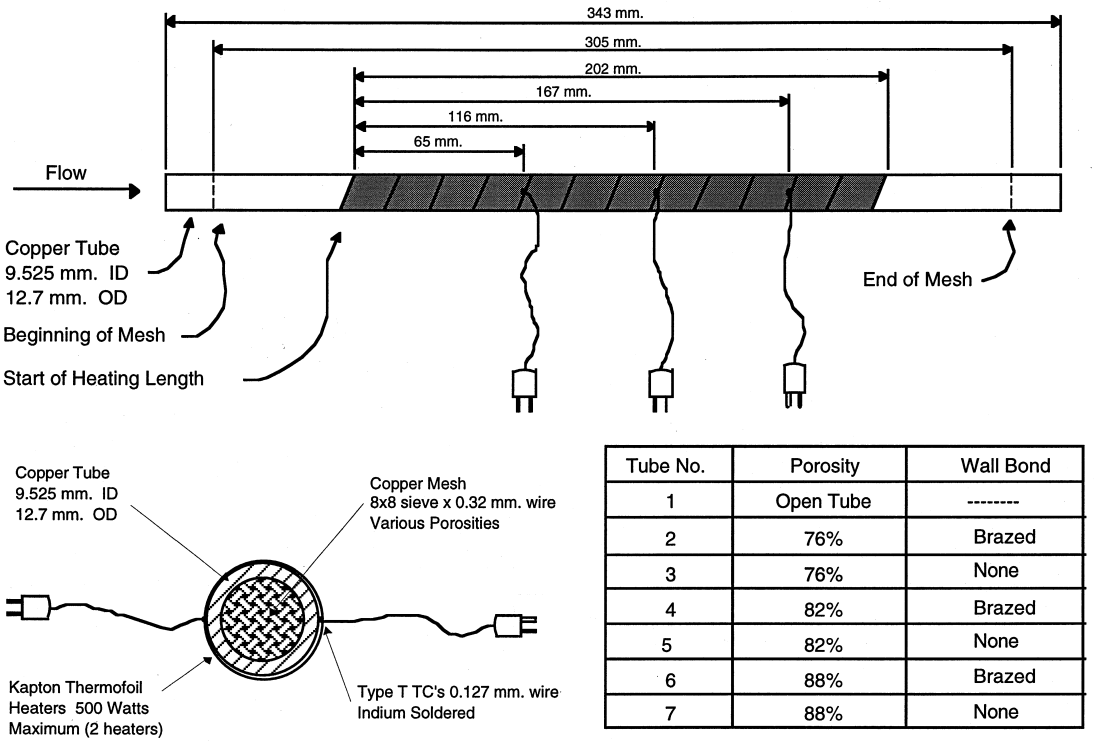

Tube No.	Porosity	Wall Bond
1	Open Tube	--------
2	76%	Brazed
3	76%	None
4	82%	Brazed
5	82%	None
6	88%	Brazed
7	88%	None

Fig. 1. Schematic of the instrumented test tube.

length is about 21 mm. The test section instrumentation includes instruments to measure mixed mean inlet and outlet temperatures and the inlet-to-outlet differential pressure drop and a precision Coriolis-effect mass-flow meter. Power input was measured using a combination of a precision shunt for current measurement and precision resistors for the voltage measurements. On all the tubes, the three TC groups, in pairs, were placed at 65 mm (2.56 in.); 116 mm (4.62 in.); and 167 mm (6.54 in.) from the start of the heated section ($x = 0$ position). These axial TC locations correspond to a flow hydraulic length of (from start of the mesh) 12.7, 17.5, and 26.5 diameters, respectively. In most cases, the heat transfer coefficient extracted at the last TC location is regarded as the representative value. The inside wall temperatures needed to calculate the local heat transfer coefficient at the thermocouple locations were obtained in the conventional manner by subtracting the calculated copper wall temperature drop from the measured outer wall temperatures under the applied uniform heat flux.

3. Experimental results

The experiments measured cryogenic heat transfer using LN2 in round copper tubes. All test tubes were placed in a horizontal configuration in this phase of the experiments. Liquid nitrogen was introduced into the test section with no sub-cooling. The total heat load applied to the test section was uniformly set at five values: 100, 200, 300, 400, and 500 W.

Tubes with a variety of porous copper-mesh inserts were tested in a progressive fashion from single-phase heat transfer to the onset of boiling and beyond. At the beginning of the particular experiment, the inlet conditions were set at the maximum mass flow rate allowed, and then the flow was gradually reduced manually in steps until steady state was reached as indicated by the test section thermocouples. This normally took a couple of minutes. At each step, a set of data was recorded. As the flow was further reduced, observation of the data indicated the following repeatable phenomenon. At the onset of boiling, the wall thermocouple ceased to rise in temperature with the reduced flow rate and even decreased slightly in some cases. This is followed by what appears to be a short plateau of sub-cooled/nucleate boiling regime. As the boiling progressed from the subcooled to the dry-out condition with further stepwise reduction in the mass flow rate, a very sudden runaway condition was indicated by the particular wall thermocouple wherever in the channel this condition was first reached. The mass flow meter reading showed a sudden dip and the pressure sensor showed a sudden rise. At this point, the mass flow rate was quickly increased manually to suppress boiling, and the experiment was terminated. In each test, in the range from the onset of boiling to the dry-out condition, it was possible to take a number of steady-state boiling data points. Thus in our test conditions, the dry-out condition in porous media heat transfer is not reached as a very sudden and unretractable occurrence from the single-phase heat transfer condition, as some studies in the literature have suggested. However, the flow range between the onset of boiling and the dry-out condition is definitely reduced compared to that for a plain tube, hence a practical wide-range does not exist where boiling can be maintained under controlled conditions.

A sample case of heat transfer data pertaining to the phenomena described above is shown in Fig. 2 for a test tube containing 82% porous non-brazed mesh subjected to a 300 W total heat load. The temperature trace indicated by the end thermocouple (node #3) is shown, on the right vertical scale, against the stepwise reduced mass flow rate in the test section. Starting at about 3.5 kg min^{-1} mass flow rate, the flow was reduced in a step fashion and shows single-phase heat transfer until about 0.8 kg min^{-1} mass flow is reached. At this mass flow point, onset of boiling (OOB) is reached as indicated by a sudden drop in the wall temperature. A narrow temperature plateau ensues with further reduction in the mass flow rate. This is the subcooled/nucleate boiling width which, with the stepwise reduction in the mass flow rate, degenerates into a rapid-voiding hence a wall temperature runaway condition. At this point, the experiment is terminated by manually increasing the mass flow rate to save the test section from a potential burn-out.

The heat transfer coefficient under node #3 corresponding to the measured temperature is also shown in Fig. 2 on the left vertical scale, which is discussed later in the text. It should be noted that, during the single-phase heat transfer tests, all the thermocouple and the flow-meter data are meaningful up to the OOB point. Hence the inlet and outlet TCs along with the flow-meter reading provide an independent check on the heat input (enthalpy rise) into the test section. Up to the OOB point, heat transfer calculations are based upon the known power input and the measured inlet temperature of single-phase LN2. Bulk fluid temperatures and inner wall temperatures at each node are calculated on this basis. Beyond the OOB point, where two-phase LN2 is present, the enthalpy rise of the fluid as determined by the inlet and outlet TCs along with the mass flow-meter reading does not match the heat input into the test section. An independent measure of fluid quality is additionally required to account for a proper heat balance. Unfortunately, a means of measuring fluid quality was not available for these experiments. Beyond the OOB point, the measured single-phase enthalpy rise along with the inlet temperature is used to determine a conservative estimate of the heat transfer. Without knowledge of the fluid quality, the known power input will lead to erroneous and sometimes negative results for the heat

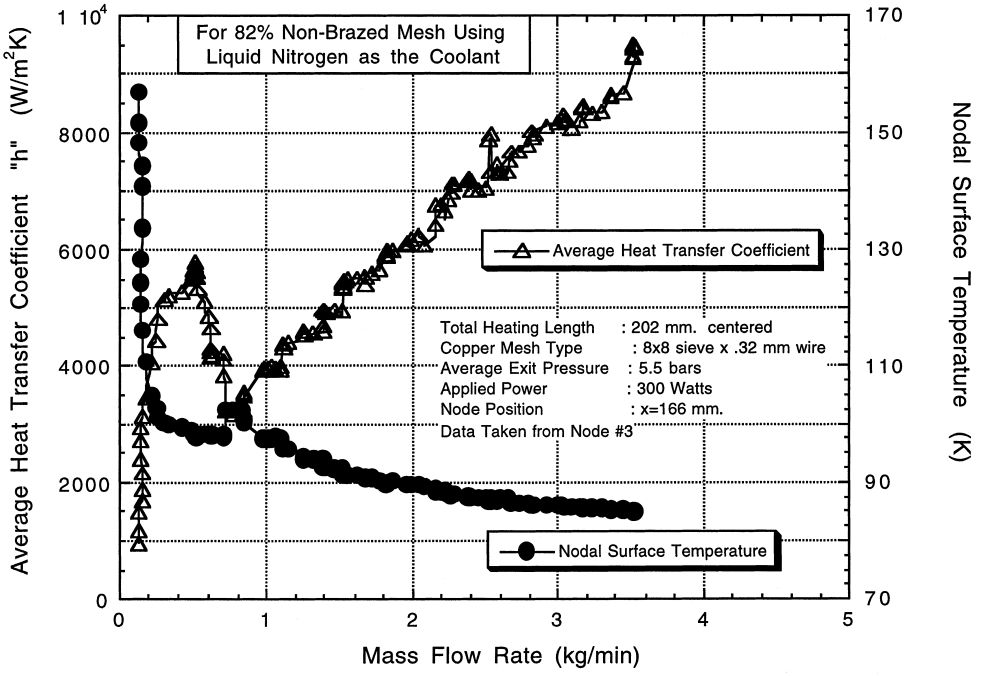

Fig. 2. Surface temperature and average heat transfer coefficient data vs mass flow for a non-brazed 82% porous mesh tube.

transfer coefficient if used in these calculations. Consequently, although plotted as read, the quantitative data from the test section should be viewed as suspect beyond the OOB point and can be useful only for trend information. A further complicating factor is the pressure regulation of the saturation temperature of LN2. The constant inlet temperature into the test section is regulated by the pressure sensor downstream of the test section. Once the boiling commences, the reading of the downstream pressure sensor is upset, and the inlet conditions cannot be kept constant. The flow-meter reading also becomes unstable and eventually faulty due to pressure fluctuations.

3.1. Pressure drop

Pressure drop data for the 9.5 mm test tubes used in the experiments are shown in Figs 3 and 4 for the single-phase LN2 flow in dimensional and non-dimensional forms, respectively. In Fig. 3, observe that the pressure drop in the tubes correlates with the square of the flow rate, both for the brazed and the non-brazed inserts. However, the pressure drop in the brazed tube, as expected, is always higher than that in the non-brazed tube at the same flow rate.

Non-dimensional pressure drop data, shown as friction coefficient versus Reynolds number, are shown in Fig. 4. Both the brazed and non-brazed data have the same slope. The complete pressure drop test data have been correlated as follows:

$$f = C\,26.8 Re^{-0.23}\,\varepsilon^{-6.29} \quad (1)$$

where C is 1.0 and 0.81 or brazed inserts for non-brazed inserts, respectively. In the tests of the non-brazed tube, the same heater tube has been used with different porous inserts. The nature of the fit is a 'snug fit' in all cases. If other fits are used, the correlation may deviate. The friction factor for the porous tubes is several orders of magnitude higher than the friction factor for the plain tube, as expected.

3.2. Heat transfer with plain tubes

The plain tube single-phase heat transfer has been measured against the traditional Sieder–Tate correlation to verify the experimental procedures for a variety of heater powers from 100 to 500 W (Fig. 5). The solid line is the Sieder–Tate heat transfer correlation for a circular plain tube. The single phase heat transfer is consistent with this correlation, with the data scatter within $\pm 5\%$.

Figure 6 presents the onset of boiling data for a 9.5 mm plain tube and the special case of the 6.4 mm plain tube. Data are shown for all the uniform heat flux test cases at various mass flow rates from less than 0.5–5 kg min^{-1}. Diversion points from the Seider–Tate curve in Fig. 5 are taken to indicate the onset of nucleate boiling

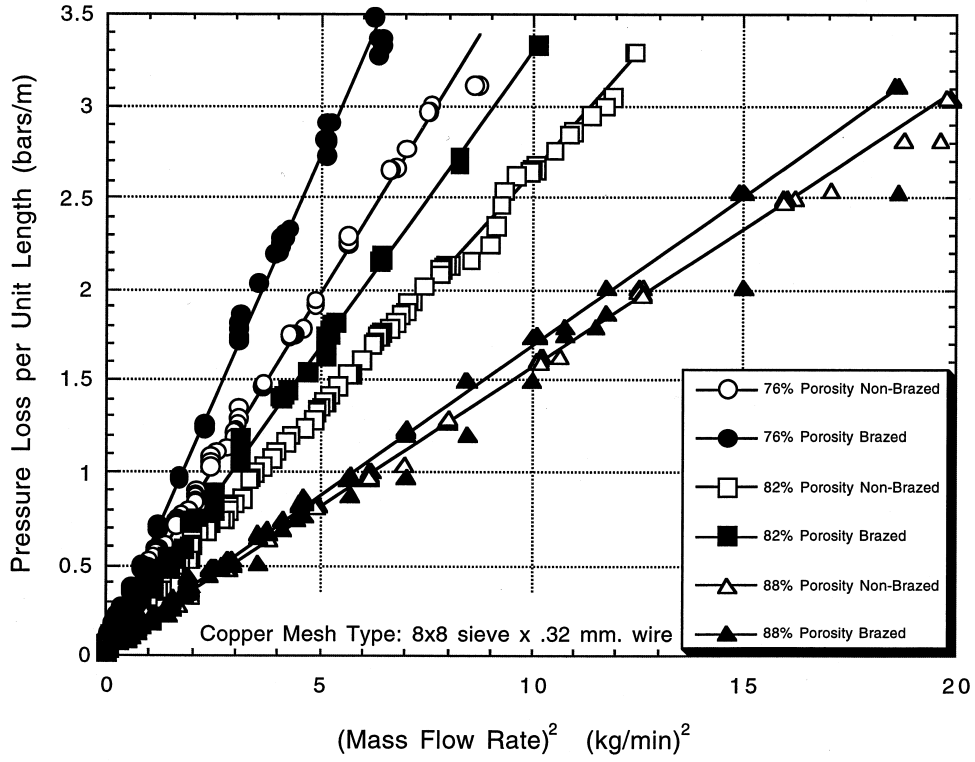

Fig. 3. Pressure loss vs mass flow rate squared for porous mesh experiments.

(ONB) in a plain tube. At the lowest heater power of 100 W, this occurs at about 0.7 kg min^{-1}. At the highest heater power test of 500 W, it occurs at about 5 kg min^{-1}. The tests of the 9.5 mm plain tube are done at 50 W total power increments. Hence the 9 data points plotted in Fig. 6 are taken at heater powers from 500 to 100 W at 50 W intervals. Because the exact location of the ONB could not be determined in the tests, correlation was tested for the two ends of the heater length. The two solid lines show the prediction of ONB using the beginning and the end of heated length as suggested in [20, 21]. Data are bracketed by the correlation band in close agreement in magnitude and trend. At mass flow rates above the ONB, heat transfer is single-phase convection. Under the ONB flow rate, it is two phase. The ONB heat flux indicated in the vertical ordinate is heat flux at the inner tube wall calculated from the measured total heater power applied via the heaters on the outside tube surface.

In the experimental program, some limited heat transfer measurements were also made with a 6 mm (0.25 in.) diameter test tube and also plotted in Fig. 6. The four data points plotted are taken at 400, 300, 200, and 100 W heater power. At 400 W, the onset of boiling occurred at about 1.8 kg min^{-1} LN2 mass flow rate and, at 100 W, the transition was noted at around 0.5 kg min^{-1}. Again data are bracketed by the ONB correlation curves using the two ends of the heater length.

Focusing on Fig. 6, one can deduce that, to support a wall heat flux level of 0.1 W mm^{-2} without boiling, one has to pass more than 6 kg min^{-1} LN2 in a 9.5 mm diameter tube. At a somewhat reduced head pressure, this is shown to be reduced significantly to about 3 kg min^{-1} for a 6 mm tube (Fig. 6). Existing correlations for the plain tube can be used confidently to determine any parameter needed for a given set of conditions. It is instructive to observe the behavior of the nodal surface temperature through ONB in the tube. Figure 7 is a composite plot of the nodal surface temperature recorded against the LN2 mass flow rates with the 9.5 mm test tube at various total heater powers. This behavior is shown for node point 2. However it is typical of all the other nodal points on the tube. For a given heater power, the nodal temperature rises as the mass flow rate of the LN2 is reduced. At a certain point, the ONB occurs indicated by an accelerated drop in the nodal temperature. The nodal temperature remains nearly constant during convective–nucleate boiling. As the mass flow rate is further reduced, a sudden temperature rise occurs at the node, which increases dramatically as the nucleate convective boiling degenerates into the critical heat flux

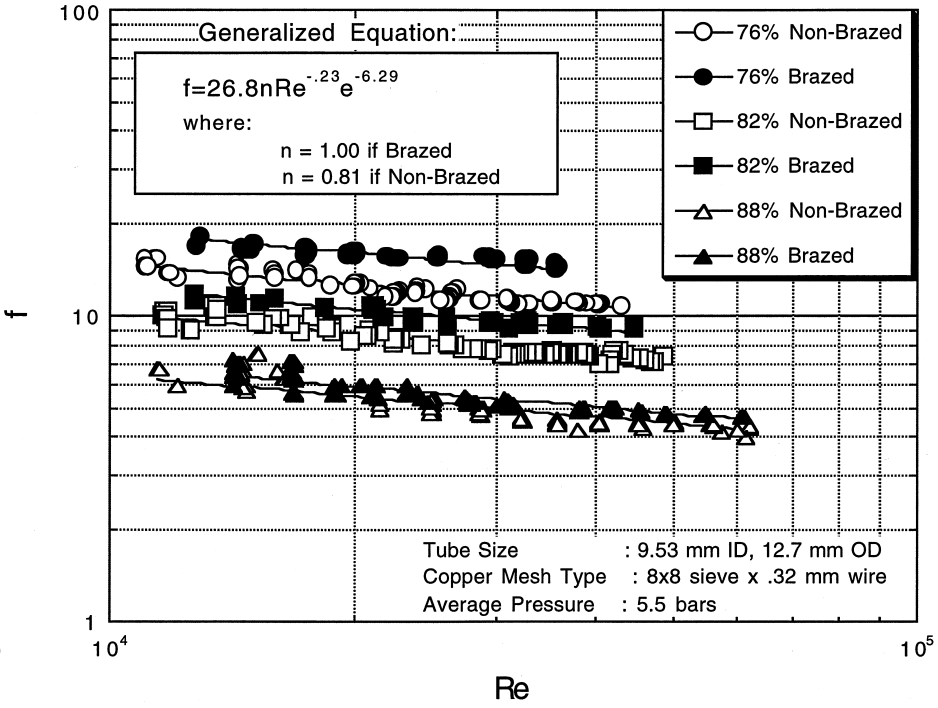

Fig. 4. Friction factor vs Reynolds number correlation for the porous mesh tube data.

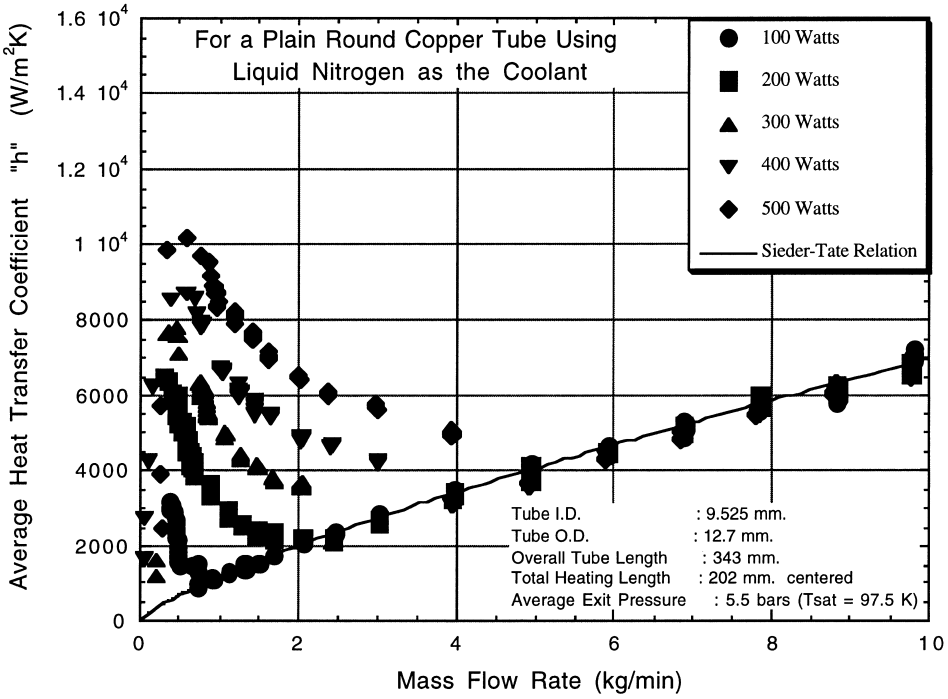

Fig. 5. Average heat transfer coefficient data vs mass flow rate for the 9.5 mm diameter plain tube at different total power levels.

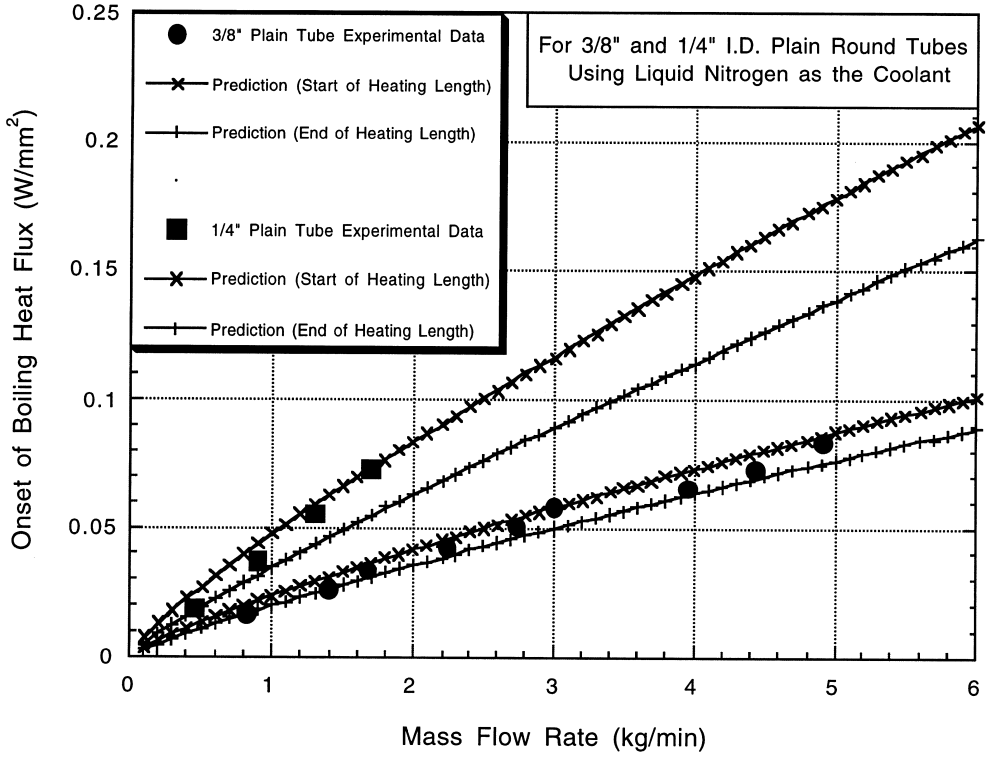

Fig. 6. Onset of boiling heat flux data vs mass flow rate for the 9.5 and 6.3 mm diameter plain test tubes and comparison with predictive correlations.

point. Tests are terminated at that point to save the experimental tubes.

Going back to Fig. 5, one can follow progression of the averaged effective heat transfer coefficient, 'h_{eff}', on the tube wall. Progression of forced convection up to the ONB point is a classic case as covered in the foregoing discussion. At and after ONB, the reduced mass flow rate enhances the heat transfer rates from the wall under the combined effect of two-phase forced convection. Hence the averaged effective heat transfer coefficient continually rises until such a point where attainment of critical heat flux causes a sudden drop in the effective h_{eff}. At which point, tests were immediately terminated to prevent tube burnout.

3.3. Heat transfer in tubes with porous conductive inserts

For the 9.5 mm diameter (3/8 in.) tube, three cases of porosity at 76, 82 and 88% have been analyzed. Figure 8 is an illustrative composite plot of the nodal temperature against the varying mass flow rate at a particular case of 300 W total heater power. The plain tube nodal temperature has also been added to provide a basis for comparative discussions.

Focusing on the particular case of 76% porosity, one can see that, as the mass flow rate is continuously reduced from 2.6 kg min^{-1} the nodal wall temperature steadily increases, as expected. At about 0.4 kg min^{-1} mass flow rate, a sudden drop in the wall temperature occurs terminating with two prominent narrow peaks followed by a very steep runaway temperature condition. The peaks indicate instability caused by the onset of boiling at this particular node location. The runaway temperature condition is the very rapid voiding condition in the porous tube after the OOB. Compared to the case of the plain tube provided in the plot, there is no prolonged convection and nucleate boiling regime plateau after the OOB. For the case of the 88% porous mesh tube, the phenomenon is similar except that the single OOB peak is well demarcated and the follow-up boiling regime is still short but a little more lingering than for the case of the 76% porous mesh tube. Hence there appears to be some porosity effect on the apparent width of the boiling plateau.

A composite plot is presented in Fig. 9 for the cases of the 76, 82 and 88% porosity mesh, for both the brazed and non-brazed tubes. The effective heat transfer coefficient, h_{eff}, has been plotted against the mass flow rate.

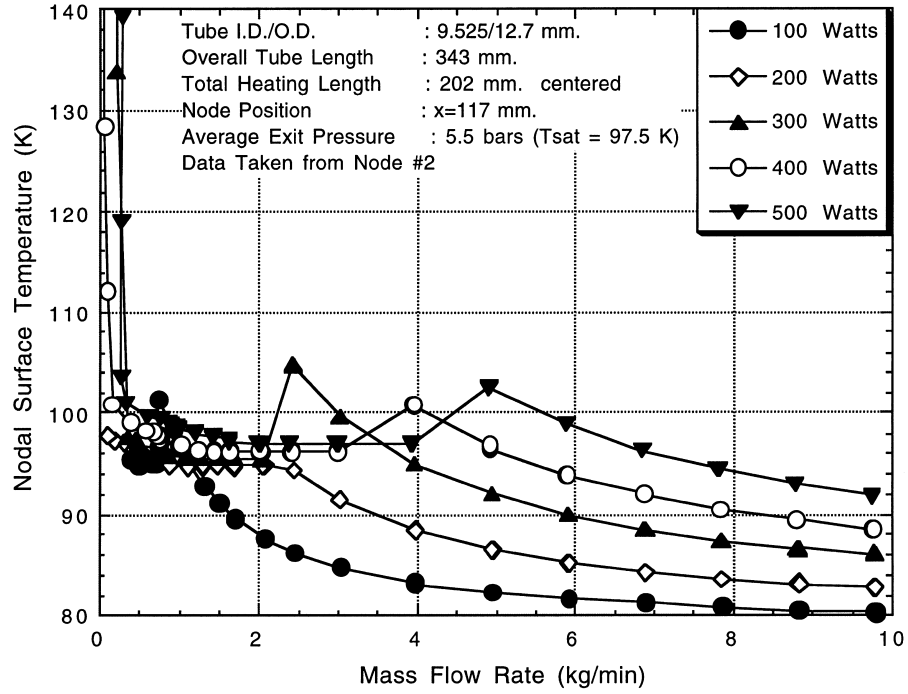

Fig. 7. Sample surface temperature data vs mass flowrate for a 9.5 mm plain test tube at various total power levels.

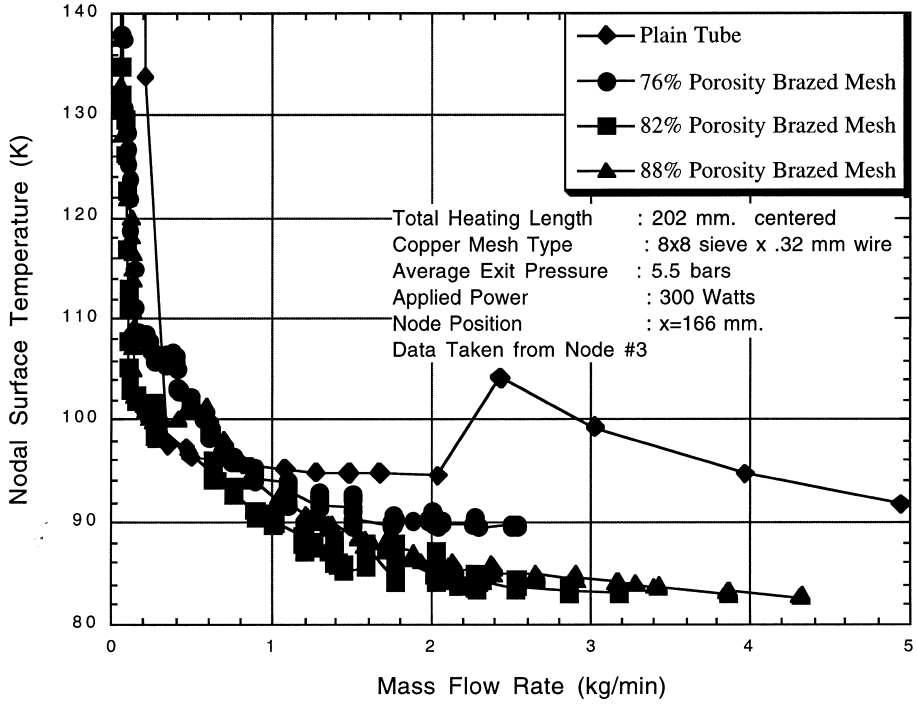

Fig. 8. Sample case of the surface temperature data vs mass flowrate for a 9.5 mm porous mesh test tube at 300 W power levels.

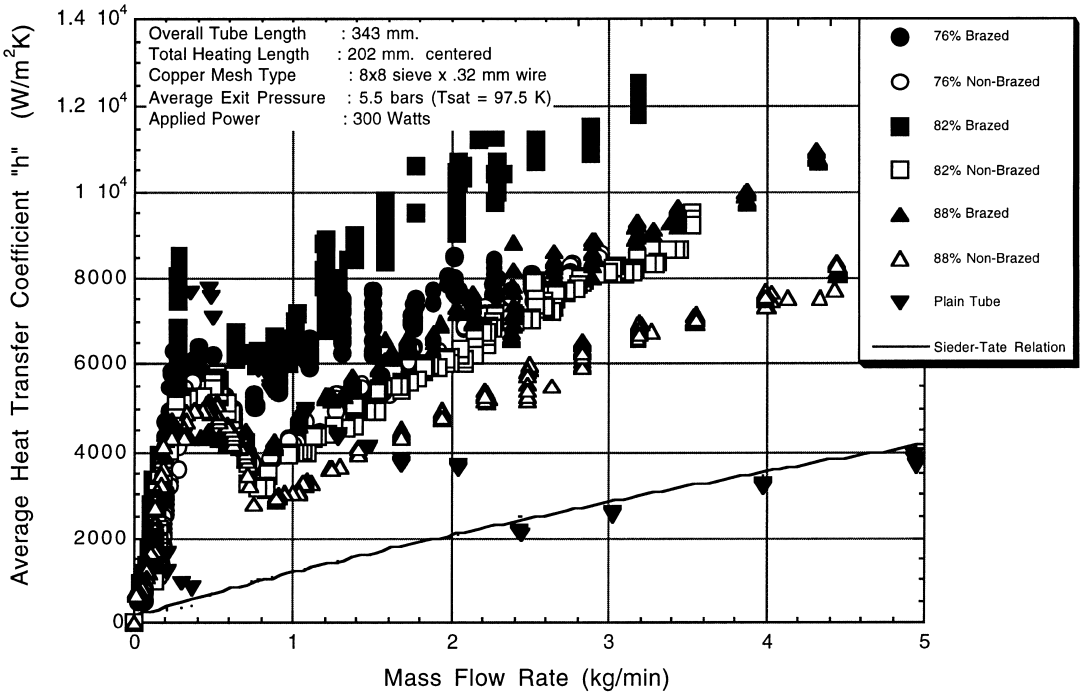

Fig. 9. Sample case of the average heat transfer coefficient data vs mass flow rate for the 9.5 mm diameter brazed mesh tube with 76% porosity at a total power level of 300 W.

As the mass flow rate of LN2 through the tube is reduced in a continuous manner at the same heater power and pressure, the heat transfer coefficient is reduced commensurate with some form of the Reynolds number dependence. At a certain point, which is typically less than 1.0 kg min^{-1} mass flow rate for all cases studied, OOB takes place that is signaled by a sharp rise in the value of h_{eff}. However, as previously indicated, a boiling instability sets in quickly as demarcated by a sharp dome. Subsequently upon a little more reduction in the mass flow rate, the critical heat flux condition is reached for these flow conditions, and there is a very sudden drop in the value of h_{eff}. This drop corresponds to the runaway wall temperature condition, at which point the test was stopped. Also shown in the same plot are the plain tube test data and the classic Sieder–Tate correlation for a circular tube. Data plots are only shown for the 300 W total heater power condition, but trends are the same for all power tests run.

Both the tubes with brazed and non-brazed porous mesh have superior heat transfer performance in single-phase LN2 cooling relative to the plain tube. Again the brazed porous mesh is superior, in all the cases, to the non-brazed porous mesh. To give some quantitative values, let us focus on 3 kg min^{-1} LN2 flow in Fig. 8. The plain tube with convective nucleate boiling seems to yield an h_{eff} of about 2800 W m^{-2} K^{-1}. For the tube with the brazed mesh h_{eff} is in the range 0.8×10^4 to 1.2×10^4 W m^{-2} K^{-1} for the three porosities tested. For the tube with the non-brazed mesh, this range is lower, about 6000 to 8000 W m^{-2} K^{-1}. Relative to a plain tube with boiling, the heat transfer enhancement attained with the porous mesh tubes is significant, i.e., up to 4-fold increased heat transfer depending on the choices made. For the three porosities tested and for the plain tubes, the highest porosity yields the lowest heat transfer enhancement. Not much difference in heat transfer effectiveness is seen between the tubes with either 76 or 82% porous mesh. But the tube with 88% porous, non-brazed mesh is seen to have decidedly lower performance. For the tubes with brazed mesh, an anomalous behavior is seen. In all the tests and at all power levels, the tube with 82% porous mesh seems to be the most effective in heat transfer. Next is the tube with 76% porous mesh, followed by the tube with 88% porous mesh.

Still another observation from Fig. 9 is that while the data for the tube with brazed mesh exhibit wider scatter, the plot of the data for the tube with non-brazed porous mesh is relatively smooth at all power levels. Smoother plots of the data for the tube with non-brazed mesh relative to the tube with brazed mesh are obvious, which is not unexpected since brazing of a porous mesh inside a tube, no matter how skillfully done, is difficult to control for uniformity especially at the wall interface. Hence an artificial but inevitable near-wall effect is introduced.

Recently, considerable analytical developments have been reported that predict heat transfer in cooling channels with porous inserts [22–25]. Particularly, reference [25] offers an extensive and successful analytical development for cylindrical channels and pressure drop, and those heat transfer results were compared with our experimental data. Excellent agreements were obtained. These results were subsequently extended to a cryogenic cooling case [26] to establish an estimate of the limits of subcooled convective boiling with LN2. Only the heuristic estimates could be provided as no fundamental work on convective boiling heat transfer in porous channels was found.

3.4. Porous medium boiling heat transfer correlations

There are no well-established heat transfer correlations for porous medium in the literature. Several tentative heat transfer correlations have been offered in the form of *Nu* vs *Pe* numbers with or without the explicit term involving porosity [27, 28]. For forms involving an explicit porosity term, *Nu* and *Pe* are based on the hydraulic diameter of the flow tube. In nonexplicit forms, *Nu* and *Pe* are formed with a characteristic pore size. Then the porosity effect is included via the definition of *Nu* and *Pe*.

Gortyshov [27, 28] offered two correlations explicitly involving the porosity effect.
With porous ceramic inserts:

$$Nu_D = 0.325 Re^{0.65}\, Pr^{0.56}\, \varepsilon^{-5.6} / {Pr_w}^{0.14} \tag{2}$$

and, with metallic foam inserts, claimed to be within 12 % error, RMS:

$$Nu_{\mathrm{d}} = 0.606 Pe^{0.56}\, \varepsilon^{-5.2} \tag{3}$$

Of these two correlations, the more relevant latter form has been checked with our experimental data. The characteristic pore size was conveniently determined from a consideration of the cross-sectional geometry of the mesh fabric rolled and pressed into the final insert to achieve the desired porosity. Resulting pore dimensions have been indicated in the figures. Repeated data fits strongly suggested that the best fit was obtained in the above form as long as the explicit porosity term was totally omitted. The porosity effect is already folded into the relationship through using characteristic pore size in defining *Nu* and *Pe*. If, however, the flow tube hydraulic diameter is used instead, then the explicit porosity term as suggested by Gorytshov was needed. The results are shown in Fig. 10 for the tubes with the non-brazed insert using both correlative forms, respectively. In either form the fit is good within $R = 97\%$ RMS.

But the data fit into correlative form is not as successful for the tubes with the brazed inserts. The best fit to the data, with a fit goodness factor of $R = 87\%$ RMS, is presented in Fig. 11 and is represented by:

$$Nu_d = 0.727 Pe^{0.467} \tag{4}$$

The larger deviation to the fit should be expected because of the larger data scatter in brazed tube tests as opposed to the data with the non-brazed tube. It is suspected that the previously alluded near-wall effects are responsible for the increased data scatter.

3.5. Heat transfer enhancement using porous mesh

Porous mesh inserts in flow channels result in large heat transfer enhancement, which has been very well established. However in cryogenic applications as in optical crystal cooling, emphasis has been shifted from enhancement level to maximum practicable flux level such that cryogenic cooling is viable without going into full voiding.

A literature review [26] revealed a very limited number of investigations that analyzed heat transfer in forced convective boiling flow in tubes/channels with porous inserts of different configurations. In chronological order, these are the investigations reported by Megerlin et al. [1], Gortyshov et al. [28] and Kuznetsov and Chikov [29]. Megerlin and coworkers investigated single-phase flow as well as forced convective boiling flow heat transfer in stainless steel tubes with stainless steel mesh and brush inserts. They reported heat transfer rates increased up to nine times in convective heat transfer in tubes with mesh inserts as compared to the case of plain tubes. They also reported that the burnout heat fluxes were 2 to 3 times the values for plain tubes for the same mass fluxes. Roizen et al. [30] reported work in which the porous inserts were made of highly permeable porous cellular porcelain. They too found that the critical heat fluxes accompanying boiling in a channel with porous inserts was 2.5–3 times higher than the values in channels with no inserts for the same mass fluxes. It should be emphasized that no such comparisons are available regarding the onset of subcooled boiling. Here emphasis is on the OOB point because, once this is reached (as demonstrated with the data in Figs 8 and 9), there is a very short operational span before the tube will be substantially voided.

Results from the test data on the OOB point heat flux versus the mass flow rate are plotted in Fig. 12 for all test tubes. Obviously, all the OOB data for the tubes with non-brazed porous inserts are almost independent of porosity. Hence reviewing a case at 1 kg min^{-1} mass flow rate, the maximum boiling heat flux is about 0.06 W mm^{-2}. The OOB for the plain tube occurs at 0.02 W mm^{-2}. The OOB heat flux for the tube with the 76% porous insert is about 0.08 W mm^{-2}. Heat transfer enhancement at OOB is at least 3-fold relative to a plain tube, in agreement with the conclusion reached by other researchers cited above and, for the tubes with 76% porosity, it is nearly a 4-fold enhancement.

A recent study examined a LN2 cooled silicon crystal using our 6.4 mm (0.25 in.) diameter porous copper inserts [17]. Seven such porous inserts mechanically

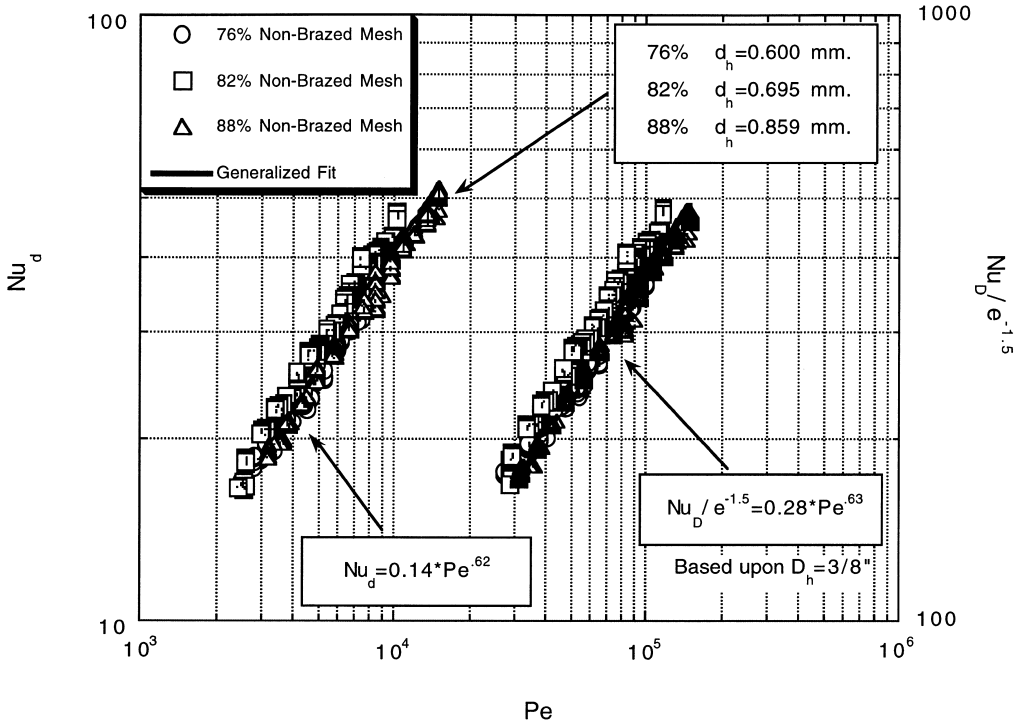

Fig. 10. Generalized *Nu* vs *Pe* correlation for the non-brazed porous mesh cases with and without the porosity effect included explicitly.

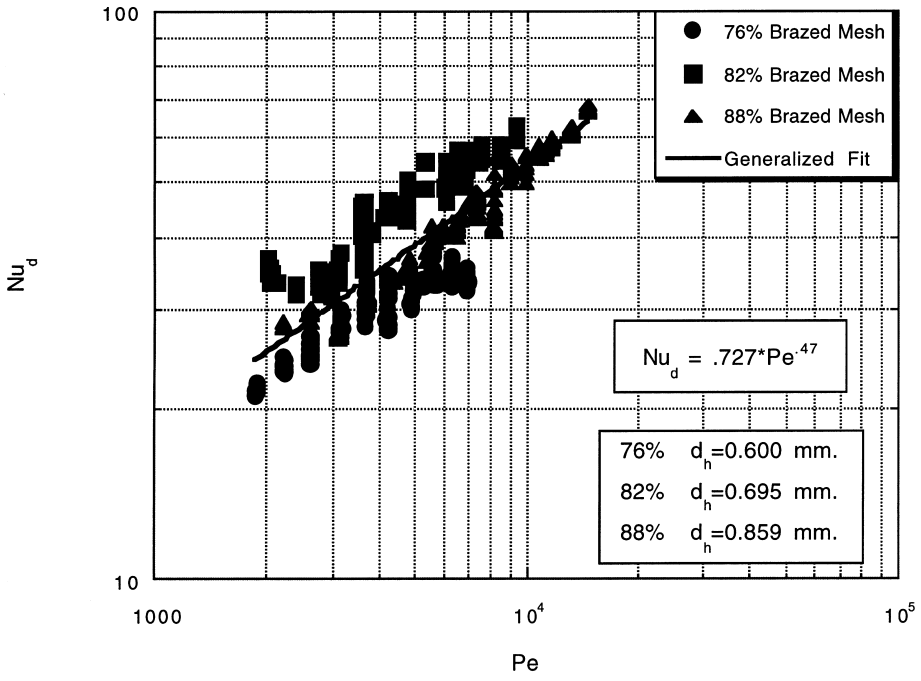

Fig. 11. Generalized *Nu* vs *Pe* correlation for the brazed porous mesh cases. *Nu* and *Pe* are formed using the calculated pore size.

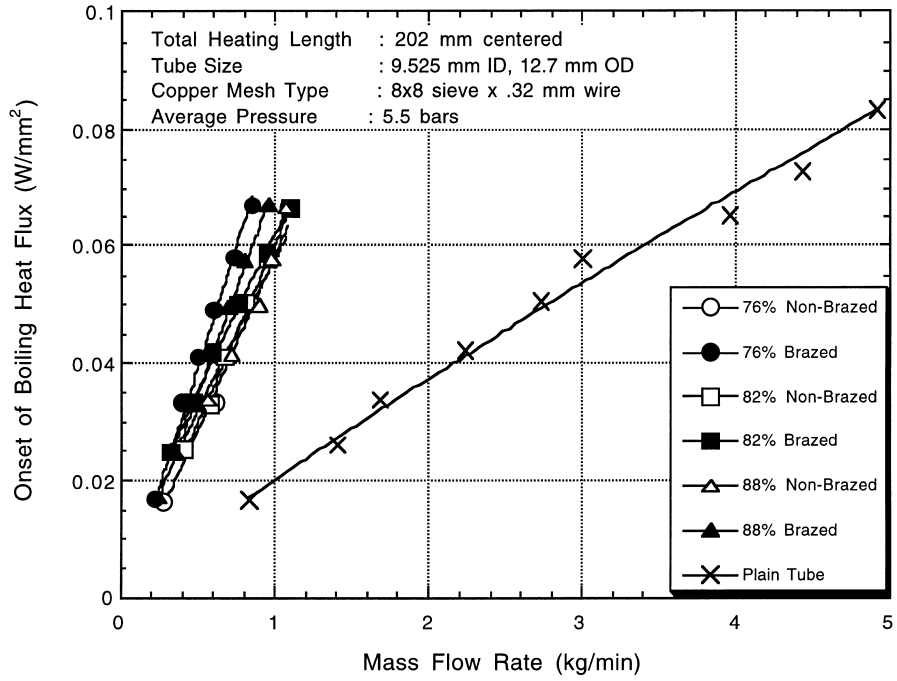

Fig. 12. Comparison of the onset of boiling (OOB) heat flux data vs mass flow rate for brazed and non-brazed mesh cases and the plain tube.

forced into the cooling channels, 60 mm long, were used to cool the crystal during an x-ray beam experiment. The data showed that, by using LN2 flow in the range 10.4–13.1 l min^{-1} for the crystal, up to 1800 W total power from the X-ray beam could be supported before ONB was detected (the monochromator absorbed at least 80 % of the incident power). The average heat flux on the surface under the beam was as high as 19 W mm^{-2}. The input data translate into an average coolant channel wall heat flux of about 1.44 W mm^{-2} and a heat transfer coefficient of about 0.26 W $cm^{-2}K^{-1}$ from the Dittus–Boelter correlation. Obviously, a significant enhancement of the heat transfer coefficient was achieved using the copper porous inserts in the 6.3 mm diameter channels to support the heat flux levels cited in the study without the OOB. The study concluded that, for the same flow rate, a cryo-cooled silicon crystal with 76% porous inserts would support a 3-fold higher total heat load compared to a crystal with plain channels before OOB was encountered (1800 W vs 600 W). In an unpublished work [26] based on the existing literature, the authors also pragmatically concluded that, with the 76% porous 9.5 mm channels, an average channel wall heat flux of about 1.42 W mm^{-2} could be supported in the subcooled boiling regime with LN2 at 13.5 l min^{-1} flow rate (9.54 kg min^{-1}). For high-precision optical work, this is of course operationally unacceptable because of the inevitable flow jitter at such high flow speeds (2.7 m s^{-1}). However, it may be acceptable in applications, which are not sensitive to flow-induced vibrations. For enhanced heat transfer with porous inserts in a 9.5 mm diameter channel, one may suggest a practical operational range of 3.2 to 4.7 kg m^{-1} LN2 flow per channel, which should support 0.8–1.0 W mm^{-2} coolant wall heat flux without the voiding concerns.

In conclusion, the tubes with non-brazed porous inserts require much higher boiling heat flux relative to a plain tube under the same operational conditions to initiate boiling. Tubes with brazed porous inserts require an even higher, up to 4-fold, increase in heat flux to initiate boiling.

4. Heat tranfer versus pressure drop

No heat transfer enhancement is complete without discussing the attendant pressure drop considerations, which are briefly addressed here. In single-phase water cooling, our engineering applications have been optimized using porous copper mesh with 76% porosity. The typical 9 mm flow channel we use has a rather larger

pressure drop, about 0.07 atm cm^{-1} at about 0.1 kg s^{-1} mass flow of deionized water (DIW). This yields significant enhancement of the convective heat transfer coefficient at about 2.8 W cm^{-2} K^{-1}. Our optimization has been driven to achieve the required heat transfer enhancement with minimal DI water rather than for minimization of the pressure drop.

In the optical element cooling case that uses a cryogen like LN2, the inherent poor heat transfer capacity and low boiling heat flux of LN2 are the primary concerns. Again maximum heat transfer enhancement is the prime consideration rather than optimization of the pumping power. Figure 13 has been plotted with this optimization criterion in mind and shows the heat transfer coefficient versus the pressure drop in a typical 9.5 mm flow channel. First, we observe that, for the same pressure drop, the tubes with brazed porous inserts will have a higher heat transfer coefficient relative to the tubes with non-brazed porous inserts. This difference is as much as 50% if curve fits were passed through the test data, which exhibit sizable scatter particularly with the brazed tubes. The relative increase in the magnitude of the heat transfer coefficient levels off at about the 2 atm m^{-1} pressure drop level. While this level of pressure drop appears to be very large in applications with long cooling channels and almost not sustainable for even subcooled LN2 operations, in real life applications, it is in fact, very usable. To give an example, in a typical application of optics cooling, a monochromator crystal will be of the order of 15 cm (6 in) long. To achieve a high effective heat transfer coefficient, say, above 1 W cm^{-2} K^{-1}, the pressure drop through the optics will be of the order of 0.3 bar.

5. Conclusions

We have examined heat transfer with liquid nitrogen in tubes that have brazed and non-brazed porous copper matrix inserts with varying porosities. The intent here has been to understand the dynamics of heat transfer and the pressure drop in porous tubes with cryogenic convective cooling.

Heat transfer experiments using LN2 as the coolant prove that the insertion of porous copper mesh into plain tubes enhances the convective heat transfer coefficient significantly. The enhancement achievable in single-phase heat transfer is virtually unlimited and totally a function of the pressure drop supportable in a particular application. However in the case of boiling, the achievable enhancement is bound by the onset of boiling (OOB) in porous tubes. Unlike the case of the plain tube, once the boiling is initiated, such tubes tend to void very rapidly with practically no sustainable margin in the nucleate boiling regime for example. In boiling, with tubes in

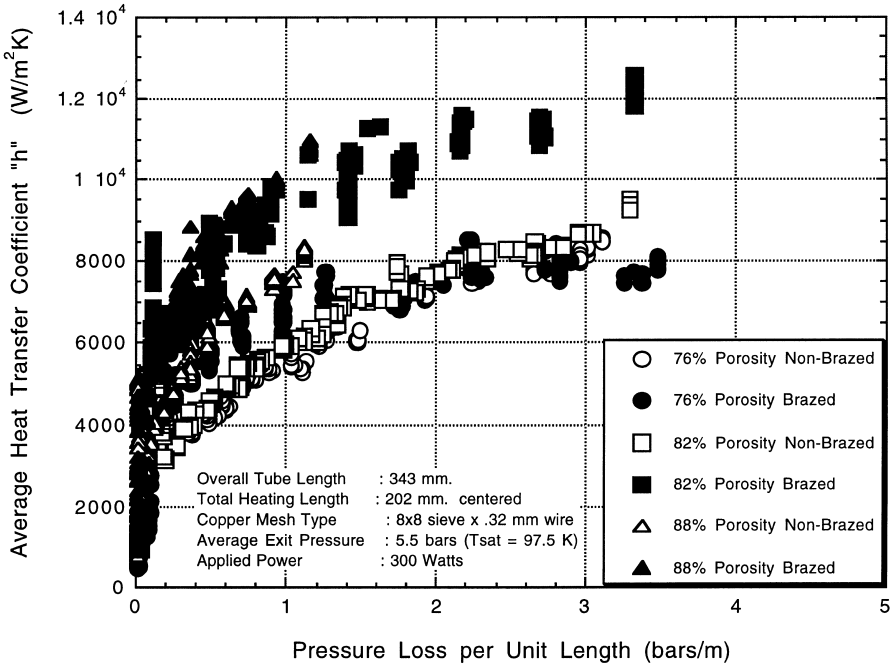

Fig. 13. The average heat transfer coefficient vs pressure loss data for the brazed and non-brazed porous tubes.

which the porous insert is brazed to the tube wall for the best thermal contact, the heat transfer enhancement is found to be on the order of 4-fold relative to a plain tube. This is of the same order of magnitude, albeit somewhat higher, than the few studies in this area had shown previously. Certainly this enhancement and the accompanying pressure drop are related to the porosity. While the lower porosity has the highest specific heat transfer enhancement; optimized against the specific pressure drop, the higher porosity tube will give a better heat transfer coefficient enhancement.

The onset of nucleate boiling (ONB) in plain tubes is found to be very predictable with the existing correlations. No such correlations exist for the tubes with porous inserts.

Porous matrix inserts offer a significant advantage in cooling, providing a jitter-free operation and a much higher effective heat transfer coefficient, at grossly reduced flow rates relative to plain tubes.

Acknowledgement

Use of the Advanced Photon Source was supported by the U.S. Department of Energy, Basic Energy Sciences, Office of Energy Research, under Contract No. W-31-109-Eng-38.

References

[1] F.E. Megerlin, R.W. Murphy, A.E. Bergles, Augmentation of heat transfer in tubes by use of mesh and brush inserts, Trans. ASME J. Heat Transfer, Vol. 96 (1974) 145–151.

[2] V.V. Apollonov, et al. Increase in the thresholds for optical failure of metallic mirror surfaces during cooling through structure with open porosity, Pis'ma Zh. Tekh. Fiz., 4 No. 19 (1978) 1193–2297.

[3] V.M. Polyaev, V.A. Maiorov, Heat exchange in a channel with porous inserts in a forced cooling system, Izv. Vyssh. Uchebn. Zaved., Mashinostr. No. 7 (1982) 51–55.

[4] V.A. Mairov, et al. Intensification of convective heat exchange in channels with porous high-thermal-conductivity filler. I. Heat exchange with local thermal equlibrium inside the permeable matrix, Inzhenerno-Fizicheskii Zhurnal, Vol. 47 (1) (1984) 13–24.

[5] V.A. Mairov, et al. Intensification of convective heat exchange in channels with porous high-thermal-conductivity filler. II. Forced heat transfer regime, Inzhenerno-Fizicheskii Zhurnal, Vol. 47(1) (1984) 199–205.

[6] V.V Apollonov, et al., Thermophysical principles of cooled laser optics based on new-type penetrable structures. Experimental heat transfer, in: R.K. Shah, E.N. Ganic, K.T. Yang, (Eds.), Fluid Mechanics and Thermodynamics, Elsevier Science Publishing Co., 1988.

[7] T.M. Kuzay, Fixed mask assembly research for advanced photon source insertion devices, ANL-90/20 (January 1990).

[8] T.M. Kuzay, J.T. Collins, A.M. Khounsary, G. Morales, Enhanced heat transfer with wool-filled tubes, ASME/JSME 3rd Joint Heat Conference, Book No. I0309E–1991 Reno, Nevada, March, 1991.

[9] Process of making cryogenically cooled high thermal performance crystal optics, U.S. Patent 5,123,982, 1992.

[10] T.M. Kuzay, Cryogenic cooling of X-ray crystals using a porous matrix, Rev. Sci. Instrum. 63 (1) (1992) Jan.

[11] G. Marot, et al., Rev. Sci. Instrum 63 (1992) 477.

[12] Lin Zhang, Cryogenic cooled silicon-based X-ray optical elements—heat transfer limit, SPIE Vol. 1997 High Heat Flux Engineering II (1993), pp. 223–229.

[13] G. Marot, Cryogenic cooling of high heat load optics, Opt. Eng., 34 (2) (1995) Feb. 426–431.

[14] B.X. Yang, et al., Performance analysis of cryogenic silicon Laue monochromators at APS undulators, SPIE Vol. 1997 High Heat Flux Engineering II (1993), pp. 302–315.

[15] G.S. Knapp, et al., A solution to the high heat loads from undulators at third generation synchrotron sources: cryogenic thin crystal monochromators, Rev. Sci. Instrum, 65 (1994) 2792.

[16] Z. Wang, et al., Thermal and deformation analysis of a cryogenically cooled silicon monochromator for high-heat-flux synchrotron sources, Rev. Sci. Instrum. 66 (2), Feb. (1995) 2267–2269.

[17] C.S. Roger, D.M. Mills, W.K. Lee, Performance of a liquid-nitrogen-cooled, thin silicon crystal monochromator on a high-power, focused wiggler synchrotron beam, Rev. Sci. Instrum 66 (6) (1995) June.

[18] C.S. Rogers, et al., Experimental results with cryogenically cooled, thin, silicon crystal X-ray monochromators on high-heat-flux beamlines, SPIE Vol. 2855 High Heat Flux Engineering III (1996), pp. 170–179.

[19] C.S. Rogers, et al., Further tests on liquid-nitrogen-cooled, thin silicon-crystal monochromators using a focused wiggler synchrotron beam, Rev. Sci. Instrum 67 (9) (1996) June.

[20] P. Van Carey, Liquid-vapor Phase-change Phenomena, Hemisphere Publishing, 1992, pp. 491–506.

[21] J.G. Collier, Convective Boiling and Condensation, McGraw-Hill, 1972.

[22] A. Nakayama, H. Koyama, F. Kuwahara, An analysis on forced convection in a channel filled with a Brinkman–Darcy porous medium: exact and approximate solution-Warme und Stoffubertragung, 23 (1988) 291–295.

[23] D.A. Nield, Effects of local thermal equilibrium in steady convective processes in a saturated porous medium: forced convection in a channel, J. of Porous Media, 1 (1998) 181–186.

[24] A. Amiri, K. Vafai, T.M. Kuzay, Effects of boundary conditions on non-darcian heat transfer through porous media and experimental comparisons, Numerical Heat Transfer: Part A, 27 (1995) 651–664.

[25] M. Sözen, T.M. Kuzay, Enhanced heat transfer in round tubes with porous insert, Int. J. Heat and Fluid Flow, 17 (2) (1996).

[26] M. Sözen, T.M. Kuzay, A study of cryo-cooling of high heat flux components by the use of cooling channels with porous inserts, Unpublished report, July 1995.

[27] Y.F. Gortyshov. G.B. Murav'ev, I.N. Nadyrov, Experimental study of flow and heat exchange in highly porous structures, Engng.-Phys. Journal 53 (1987) 357.

[28] Y.F. Gortyshov, I.N. Nadyrov, S.R. Ashikmin, A.P. Kunevich, Heat transfer in the flow of a single-phase and boiling coolant in a channel with a porous insert, J. Engineering Physics and Thermophysics (trans. from Russian), 60 (2) (1991) 202–207.
[29] V.V. Kuznetsov, S.B. Chikov, Heat transfer under conditions of flow along a fuel element placed in a porous medium, High Temperature (trans. from Russian), 31 (2) (1993) 242–246.
[30] L.I. Roizen, D.G. Rachitskii, I.R. Rubin, L.M. Vertogradskaya, L.A. Yudina, M.B. Pypkina, Heat transfer with boiling of nitrogen and Freon-113 on porous metallic coatings, High Temperature (trans. from Russian) 20 (2) (1982) 264–270.